

ADAPTIVE BAYESIAN CHANNEL GAIN CARTOGRAPHY

Donghoon Lee, Dimitris Berberidis, and Georgios B. Giannakis

Dept. of ECE and Digital Technology Center, University of Minnesota, USA

Emails: {leex6962, bermp001, georgios}@umn.edu

ABSTRACT

Channel gain cartography relies on sensor measurements to construct maps providing the attenuation profile between arbitrary transmitter-receiver locations. Existing approaches capitalize on tomographic models, where shadowing is the weighted integral of a spatial loss field (SLF) depending on the propagation environment. Currently, the SLF is learned via regularization methods tailored to the propagation environment. However, the effectiveness of existing approaches remains unclear especially when the propagation environment involves heterogeneous characteristics. To cope with this, the present work considers a piecewise homogeneous SLF with a hidden Markov random field (MRF) model under the Bayesian framework. Efficient field estimators are obtained by using samples from Markov chain Monte Carlo (MCMC). Furthermore, an uncertainty sampling algorithm is developed to adaptively collect measurements. Real data tests demonstrate the capabilities of the novel approach.

Index Terms— channel gain cartography, radio tomography, Markov chain Monte Carlo, active learning

1. INTRODUCTION

Based on the measurements collected by a network of spatially distributed sensors, channel gain cartography constructs maps providing channel-state information for links between locations where no sensors are present [1]. Such maps can be employed in cognitive radio setups to control the interference that the secondary network inflicts to primary users that do not transmit – setup encountered with television broadcast systems [2, 3, 4, 5]. The non-collaborative nature of these primary users precludes any direct form of channel estimation between secondary transmitters and primary receivers.

Existing methods for channel gain cartography build upon the intuitive principle that spatially close radio links exhibit similar shadowing [6]. Most of these methods adopt a tomographic approach [7], where shadowing attenuation is modeled as the weighted integral of an unknown spatial loss field (SLF) capturing the absorption induced by objects located in the propagation medium [7, 8, 9, 10, 11]. The weights

in the integral are determined by a function depending on the transmitter-receiver locations that is either selected based on heuristic criteria [7, 12], or blindly learned via the non-parametric kernel regression method [13]. A channel map can thus be obtained once the SLF has been estimated.

Conventionally, the SLF is learned via regularized least-squares (LS) methods tailored to the propagation environment [11, 12, 14]. However, those approaches are less effective when the propagation environment exhibits heterogeneous characteristics. Different from past works, the present one leverages the Bayesian framework to learn the piecewise homogeneous SLF through a hidden Markov random field (MRF) model [15], which captures spatial correlations of neighboring regions exhibiting related statistical behavior. Efficient field estimators will be derived by using Markov chain Monte Carlo (MCMC) sampling [16], which is a powerful tool for Bayesian inference when the analytical solutions of the minimum mean-square error (MMSE) or the maximum a posteriori (MAP) estimators are not available. Furthermore, an adaptive data acquisition method will be developed, with the goal of reducing uncertainty of the SLF.

Notation: \mathbf{I}_n is the $n \times n$ identity matrix. Superscript $^\top$ represents transposition. $|\cdot|$ stands for a cardinality of the set.

2. MODEL AND PROBLEM STATEMENT

Consider a set of sensors deployed over a two-dimensional geographical area indexed by a set $\mathcal{A} \subset \mathbb{R}^2$. After averaging out small-scale fading effects, the channel gain measurement over a link between a transmitter located at $\mathbf{x} \in \mathcal{A}$ and a receiver located at $\mathbf{x}' \in \mathcal{A}$ can be represented (in dB) as

$$g(\mathbf{x}, \mathbf{x}') = g_0 - \gamma 10 \log_{10} d(\mathbf{x}, \mathbf{x}') - s(\mathbf{x}, \mathbf{x}') \quad (1)$$

where g_0 is the path gain at unit distance; $d(\mathbf{x}, \mathbf{x}') := \|\mathbf{x} - \mathbf{x}'\|_2$ is the distance between the transceivers at \mathbf{x} and \mathbf{x}' ; γ is the pathloss exponent; and $s(\mathbf{x}, \mathbf{x}')$ is the attenuation due to shadow fading. In CG cartography, a tomographic model for the shadow fading is adopted [7, 12, 11], namely

$$s(\mathbf{x}, \mathbf{x}') \simeq \sum_{i=1}^{N_g} w(\mathbf{x}, \mathbf{x}', \tilde{\mathbf{x}}_i) f(\tilde{\mathbf{x}}_i). \quad (2)$$

where $\{\tilde{\mathbf{x}}_i\}_{i=1}^{N_g}$ is a grid of points over \mathcal{A} , $f: \mathcal{A} \rightarrow \mathbb{R}$ denotes the *spatial loss field* (SLF) capturing the attenuation at each location, and $w(\mathbf{x}, \mathbf{x}', \tilde{\mathbf{x}})$ is the weight function modeling the

The work in this paper was supported by NSF grants 1343248, 1442686, 1508993, and 1509040.

influence of the SLF at $\tilde{\mathbf{x}}$ to the shadowing experienced by link $\mathbf{x}-\mathbf{x}'$. Examples of the weight function include the *normalized ellipse model* taking the form [14]

$$w(\mathbf{x}, \mathbf{x}', \tilde{\mathbf{x}}) := \begin{cases} 1/\sqrt{d(\mathbf{x}, \mathbf{x}')}, & \text{if } d(\mathbf{x}, \tilde{\mathbf{x}}) + d(\mathbf{x}', \tilde{\mathbf{x}}) \\ & < d(\mathbf{x}, \mathbf{x}') + \lambda \\ 0, & \text{otherwise} \end{cases} \quad (3)$$

where $\lambda > 0$ is a tunable parameter. The value of λ is commonly set to half the wavelength to assign non-zero weights only within the first Fresnel zone. Overall, the model in (2) shows how the nature and spatial distribution of obstructions in the propagation medium influence the attenuation between a pair of locations.

To estimate the channel gain map, N sensors located at $\{\mathbf{x}_1, \dots, \mathbf{x}_N\} \in \mathcal{A}$ collaboratively obtain channel gain measurements. At time slot t , the radios indexed by $n(t)$ and $n'(t)$ measure the channel gain $g_t := g(\mathbf{x}_{n(t)}, \mathbf{x}_{n'(t)})$ by exchanging pilot sequences, where $n(t), n'(t) \in \{1, \dots, N\}$. It is supposed that g_0 and γ have been estimated during a calibration phase. After subtracting these from g_t , the shadowing estimate $\tilde{s}_t := \tilde{s}(\mathbf{x}_{n(t)}, \mathbf{x}_{n'(t)}) := s(\mathbf{x}_{n(t)}, \mathbf{x}_{n'(t)}) + \nu_t$ is obtained, where ν_t denotes measurement noise. Given those measurement $\tilde{\mathbf{s}}_t := [\tilde{s}_1, \dots, \tilde{s}_t]^\top \in \mathbb{R}^t$ along with the known set of links $\{(\mathbf{x}_{n(\tau)}, \mathbf{x}_{n'(\tau)})\}_{\tau=1}^t$ and the weight function w , the problem is to estimate $g(\mathbf{x}, \mathbf{x}')$ between any pair of locations $(\mathbf{x}, \mathbf{x}') \in \mathcal{A}$. To this end, it suffices to estimate f , or equivalently $\mathbf{f} := [f(\tilde{\mathbf{x}}_1), \dots, f(\tilde{\mathbf{x}}_{N_g})]^\top \in \mathbb{R}^{N_g}$. Afterwards, the arbitrary channel gain $g(\mathbf{x}, \mathbf{x}')$ can be obtained by substituting (2) into (1) and replacing f with its estimate.

3. ADAPTIVE BAYESIAN CG CARTOGRAPHY

In this section, we propose a two-layer Bayesian model for the SLF, as well as, an MCMC-based approach for inference. Furthermore, an adaptive data acquisition strategy to select informative measurements is introduced.

3.1. Field estimation via Markov chain Monte Carlo

Let \mathcal{A} consist of two disjoint homogeneous regions $\mathcal{A}_0 := \{\mathbf{x} | \mathbb{E}[f(\mathbf{x})] = \mu_{f_0}, \text{Var}[f(\mathbf{x})] = \sigma_{f_0}^2, \mathbf{x} \in \mathcal{A}\}$ and $\mathcal{A}_1 := \{\mathbf{x} | \mathbb{E}[f(\mathbf{x})] = \mu_{f_1}, \text{Var}[f(\mathbf{x})] = \sigma_{f_1}^2, \mathbf{x} \in \mathcal{A}\}$, giving rise to a hidden label field $\mathbf{z} := [z(\tilde{\mathbf{x}}_1), \dots, z(\tilde{\mathbf{x}}_{N_g})]^\top \in \{0, 1\}^{N_g}$ of binary labels with $z(\tilde{\mathbf{x}}_i) = k$ if $\tilde{\mathbf{x}}_i \in \mathcal{A}_k \forall i$, and $k = 0, 1$. We then model the conditional distribution of $f(\tilde{\mathbf{x}}_i)$ as

$$f(\tilde{\mathbf{x}}_i) | z(\tilde{\mathbf{x}}_i) = k \sim \mathcal{N}(\mu_{f_k}, \sigma_{f_k}^2), \quad (4)$$

while the Ising prior [17], which is a binary version of the discrete MRF Potts prior [15], is assigned to \mathbf{z} to capture the dependency among spatially correlated labels. By the Hammersley-Clifford theorem [18], the Ising prior of \mathbf{z} follows a Gibbs distribution

$$p(\mathbf{z} | \beta) = \frac{1}{C(\beta)} \exp \left[\beta \sum_{i=1}^{N_g} \sum_{j \in \mathcal{N}(\tilde{\mathbf{x}}_i)} \delta(z(\tilde{\mathbf{x}}_j) = z(\tilde{\mathbf{x}}_i)) \right] \quad (5)$$

where $\mathcal{N}(\tilde{\mathbf{x}}_i)$ is a set of indices associated with 1-hop neighbors of $\tilde{\mathbf{x}}_i$ on the rectangular grid, β is the granularity coefficient to control the degree of homogeneity in \mathbf{z} , $\delta(\cdot)$ is the Kronecker delta function, and $C(\beta) := \sum_{\mathbf{z} \in \mathcal{Z}} \exp \left[\beta \sum_{i=1}^{N_g} \sum_{j \in \mathcal{N}(\tilde{\mathbf{x}}_i)} \delta(z(\tilde{\mathbf{x}}_j) = z(\tilde{\mathbf{x}}_i)) \right]$ is the partition function with $\mathcal{Z} := \{0, 1\}^{N_g}$. By assuming conditional independence of $\{f(\tilde{\mathbf{x}}_i)\}_{i=1}^{N_g}$ given \mathbf{z} , the resulting model is referred to as the Gauss-Potts model [19] with two labels.

Let ν_t be independent and identically distributed (i.i.d) Gaussian with zero mean and variance σ_{ν}^2 , and $\boldsymbol{\theta}$ denote the known parameter vector including σ_{ν}^2 , β , and $\boldsymbol{\theta}_f := [\mu_{f_0}, \mu_{f_1}, \sigma_{f_0}^2, \sigma_{f_1}^2]^\top$. The weight matrix $\mathbf{W}_t \in \mathbb{R}^{N_g \times t}$ is constructed with columns equal to $\mathbf{w}_\tau := [w(\mathbf{x}_{n(\tau)}, \mathbf{x}_{n'(\tau)}, \tilde{\mathbf{x}}_1), \dots, w(\mathbf{x}_{n(\tau)}, \mathbf{x}_{n'(\tau)}, \tilde{\mathbf{x}}_{N_g})]^\top \in \mathbb{R}^{N_g}$ of the link $\mathbf{x}_{n(\tau)}-\mathbf{x}_{n'(\tau)}$ for $\tau = 1, \dots, t$. Then, one can cast Bayesian CG cartography by writing the joint posterior as

$$p(\mathbf{f}, \mathbf{z}, \boldsymbol{\theta} | \tilde{\mathbf{s}}_t) \propto p(\tilde{\mathbf{s}}_t | \mathbf{f}, \sigma_{\nu}^2) p(\mathbf{f} | \mathbf{z}, \boldsymbol{\theta}_f) p(\mathbf{z} | \beta) p(\boldsymbol{\theta}), \quad (6)$$

where $p(\tilde{\mathbf{s}}_t | \mathbf{f}, \sigma_{\nu}^2) \sim \mathcal{N}(\mathbf{W}_t^\top \mathbf{f}, \sigma_{\nu}^2 \mathbf{I}_t)$ is the likelihood, and $p(\mathbf{f} | \mathbf{z}, \boldsymbol{\theta}_f)$, $p(\mathbf{z} | \beta)$, and $p(\boldsymbol{\theta})$ are the priors of $\{\mathbf{f}, \mathbf{z}, \boldsymbol{\theta}\}$, respectively. By utilizing the posterior in (6), the MMSE estimator of \mathbf{f} is found as $\hat{\mathbf{f}}_{\text{MMSE}} := \mathbb{E}[\mathbf{f} | \mathbf{z} = \hat{\mathbf{z}}_{\text{MAP}}, \tilde{\mathbf{s}}_t]$, where \mathbf{z} is fixed to the marginal MAP estimate of \mathbf{z} , i.e., $\hat{\mathbf{z}}_{\text{MAP}} = \arg \max_{\mathbf{z}} p(\mathbf{z} | \tilde{\mathbf{s}}_t)$.

Although the suggested estimators have been advocated [20, 21], analytical solutions are not available due to the complex form of the posterior in (6) for marginalization or maximization. To bypass this challenge, one can use samples generated from the posterior in (6) as its proxy and then numerically obtain the desired estimators from those samples. MCMC is a class of algorithms to generate samples from a complex distribution [16]. Among MCMC methods, Gibbs sampling is particularly suitable for this work. It draws samples following the target distribution (e.g., the posterior in (6)) by sweeping through each variable to sample from its conditional distribution while fixing the others to their up-to-date values. Although the samples at early iterations of Gibbs sampling with random initialization are not representative of the desired distribution (such duration is called the *burn-in* period N_{Burn}), the theory of MCMC guarantees that the stationary distribution of those samples is matched with the target distribution [16].

Gibbs sampling requires only the proportionality of the conditional distribution, as described in Alg. 1. Particularly for the posterior conditional of \mathbf{f} , it is easy to show

$$p(\mathbf{f} | \tilde{\mathbf{s}}_t, \mathbf{z}, \boldsymbol{\theta}) \propto p(\tilde{\mathbf{s}}_t | \mathbf{f}, \sigma_{\nu}^2) p(\mathbf{f} | \mathbf{z}, \boldsymbol{\theta}_f) \sim \mathcal{N}(\tilde{\boldsymbol{\mu}}_{f|z}, \boldsymbol{\Sigma}_{f|z}), \quad (7)$$

where

$$\boldsymbol{\Sigma}_{f|z} := \left((\sigma_{\nu}^2)^{-1} \mathbf{W}_t \mathbf{W}_t^\top + \boldsymbol{\Delta}_{f|z}^{-1} \right)^{-1} \quad (8)$$

$$\tilde{\boldsymbol{\mu}}_{f|z} := \boldsymbol{\Sigma}_{f|z} \left((\sigma_{\nu}^2)^{-1} \mathbf{W}_t \tilde{\mathbf{s}}_t + \boldsymbol{\Delta}_{f|z}^{-1} \boldsymbol{\mu}_{f|z} \right) \quad (9)$$

since $p(\mathbf{f} | \mathbf{z}, \boldsymbol{\theta}_f)$ follows $\mathcal{N}(\boldsymbol{\mu}_{f|z}, \boldsymbol{\Delta}_{f|z})$ by (4), with $\boldsymbol{\mu}_{f|z} := \mathbb{E}[\mathbf{f} | \mathbf{z}]$ and $\boldsymbol{\Delta}_{f|z} := \text{diag}(\{\text{Var}[f_i | z_i]\}_{i=1}^{N_g})$ with $f_i :=$

Algorithm 1 Generic Gibbs sampler for \mathbf{f} and \mathbf{z}

Input: $\mathbf{z}^{(0)}$, $\boldsymbol{\theta}$, $\tilde{\mathbf{s}}_t$, N_{Burn} , and N_{Iter} .

- 1: **for** $l = 1$ to N_{Iter} **do**
 - 2: Generate $\mathbf{f}^{(l)} \sim p(\mathbf{f}|\tilde{\mathbf{s}}_t, \mathbf{z}^{(l-1)}, \boldsymbol{\theta})$ in (7)
 - 3: Generate $\mathbf{z}^{(l)} \sim p(\mathbf{z}|\tilde{\mathbf{s}}_t, \mathbf{f}^{(l)}, \boldsymbol{\theta})$ via Alg. 2
 - 4: **end for**
 - 5: **return** $\mathcal{S} := \{\mathbf{f}^{(l)}, \mathbf{z}^{(l)}\}_{l=N_{\text{Burn}}+1}^{N_{\text{Iter}}}$
-

$f(\tilde{\mathbf{x}}_i)$ and $z_i := z(\tilde{\mathbf{x}}_i)$. Hence, \mathbf{f} can be easily simulated by a standard sampling method. On the other hand, another Gibbs sampler is required to simulate $p(\mathbf{z}|\tilde{\mathbf{s}}_t, \mathbf{f}, \boldsymbol{\theta}) \propto p(\mathbf{f}|\mathbf{z}, \boldsymbol{\theta}_f)p(\mathbf{z}|\beta)$ to avoid the intractable computation of $C(\beta)$ in (5). Let \mathbf{z}_{-i} and $\mathbf{z}_{\mathcal{N}(\tilde{\mathbf{x}}_i)}$ represent replicas of \mathbf{z} without its i -th entry, and only with the entries of $\mathcal{N}(\tilde{\mathbf{x}}_i)$, respectively. By the Markovianity of \mathbf{z} and conditional independence between f_i and $f_j \forall i \neq j$ given \mathbf{z} , the conditional distribution of z_i is given by

$$p(z_i|\mathbf{z}_{-i}, \tilde{\mathbf{s}}_t, \mathbf{f}, \boldsymbol{\theta}) \propto \exp \left[\ell(z_i) + \beta \sum_{j \in \mathcal{N}(\tilde{\mathbf{x}}_i)} \delta(z_j = z_i) \right] \quad (10)$$

where $\ell(z_i) := \ln p(f_i|z_i, \boldsymbol{\theta}_f)$. After evaluating (10) for $z_i = 0, 1$ and normalizing, one can obtain $p(z_i = 1|\mathbf{z}_{-i}, \tilde{\mathbf{s}}_t, \mathbf{f}, \boldsymbol{\theta}) = (1 + h_i)^{-1}$, where

$$h_i := \exp \left[\ell(z_i = 0) - \ell(z_i = 1) + \sum_{j \in \mathcal{N}(\tilde{\mathbf{x}}_i)} \beta(1 - 2z_j) \right] \quad (11)$$

with $\delta(z_j = 0) - \delta(z_j = 1) = 1 - 2z_j$. Then, the sample of \mathbf{z} can be obtained via the single-site Gibbs sampler by using (11), as summarized in Alg. 2.

Building on [20], the elementwise MAP estimator of \mathbf{z} and its sample-based approximation are

$$\begin{aligned} \hat{z}_{i,\text{MAP}} &= \arg \max_{z_i \in \{0,1\}} p(z_i|\tilde{\mathbf{s}}_t) \\ &\simeq \arg \max_{z_i \in \{0,1\}} \frac{1}{|\mathcal{S}|} \sum_{l=N_{\text{Burn}}+1}^{N_{\text{Iter}}} \delta(z_i^{(l)} = z_i) \end{aligned} \quad (12)$$

for $i = 1, \dots, N_g$. After obtaining $\hat{\mathbf{z}}_{\text{MAP}}$, the sample-based elementwise MMSE estimator of \mathbf{f} similarly follows as

$$\hat{f}_{i,\text{MMSE}} \simeq \frac{1}{|\mathcal{S}_i|} \sum_{l=N_{\text{Burn}}+1}^{N_{\text{Iter}}} f_i^{(l)} \delta(z_i^{(l)} = \hat{z}_{i,\text{MAP}}), \quad \forall i, \quad (13)$$

where $\mathcal{S}_i \subset \mathcal{S}$ is a subset of samples such that $z_i^{(l)} = \hat{z}_{i,\text{MAP}}$ for $l = N_{\text{Burn}} + 1, \dots, N_{\text{Iter}}$.

3.2. Adaptive data acquisition via uncertainty sampling

The proposed Bayesian CG cartography accounts for the uncertainty of \mathbf{f} , through the variance in (8). Therefore, one can adaptively collect a measurement (or a mini-batch of measurements) when a set of available sensing radio pairs are revealed, with the goal of reducing the uncertainty of \mathbf{f} . Note that the resulting sampling algorithm has been studied under the name of active learning [22] in the machine learning community. To this end, the conditional entropy [23] is considered as an uncertainty measure of \mathbf{f} at time slot t , namely,

Algorithm 2 Single-site Gibbs sampler for \mathbf{z}

Input: $\mathbf{f}^{(l)}$ and $\mathbf{z}^{(l-1)}$

- 1: Initialize $\zeta^{(l)} = \mathbf{z}^{(l-1)}$
 - 2: **for** $i = 1$ to N_g **do**
 - 3: Obtain h_i in (11) with $\mathbf{z} = \zeta^{(l)}$ and $\mathbf{f} = \mathbf{f}^{(l)}$
 - 4: **if** $u \sim \mathcal{U}_{(0,1)} < (1 + h_i)^{-1}$ **then**
 - 5: Set $\zeta_i^{(l)} = 1$
 - 6: **else**
 - 7: Set $\zeta_i^{(l)} = 0$
 - 8: **end if**
 - 9: **end for**
 - 10: **return** $\mathbf{z}^{(l)} = \zeta^{(l)}$
-

Algorithm 3 Adaptive Bayesian CG cartography

Input: $\mathbf{z}^{(0)}$, $\tilde{\mathbf{s}}_0$, $\boldsymbol{\theta}$, N_{Burn} , N_{Iter} , g_0 and γ .

- 1: **for** $\tau = 0, 1, \dots$ **do**
 - 2: Obtain $\mathcal{S}^{(\tau)}$ via Alg. 1 ($\mathbf{z}^{(0)}$, $\boldsymbol{\theta}$, $\tilde{\mathbf{s}}_\tau$, N_{Burn} , N_{Iter})
 - 3: Obtain $\hat{\mathbf{z}}_{\text{MAP}}^{(\tau)}$ from (12) by using $\mathcal{S}^{(\tau)}$
 - 4: Obtain $\hat{\mathbf{f}}_{\text{MMSE}}^{(\tau)}$ from (13) by using $\hat{\mathbf{z}}_{\text{MAP}}^{(\tau)}$ and $\mathcal{S}^{(\tau)}$
 - 5: Calculate $\bar{u}(\mathbf{w})$ in (16) for $\mathbf{w} \in \mathcal{W}_{\tau+1}$ by using $\mathcal{S}^{(\tau)}$
 - 6: Collect $\tilde{\mathbf{s}}_{\tau+1}$ from sensors associated with max $\bar{u}(\mathbf{w})$
 - 7: Set $\tilde{\mathbf{s}}_{\tau+1} = [\tilde{\mathbf{s}}_\tau^\top, \tilde{\mathbf{s}}_{\tau+1}^\top]^\top$ and $\mathbf{z}^{(0)} = \hat{\mathbf{z}}_{\text{MAP}}^{(\tau)}$
 - 8: **end for**
 - 9: Consider arbitrary locations $\{\mathbf{x}, \mathbf{x}'\} \in \mathcal{A}$
 - 10: Estimate $\hat{s}(\mathbf{x}, \mathbf{x}')$ via (2) by using $\hat{\mathbf{f}}_{\text{MMSE}}^{(\tau)}$
 - 11: Estimate $\hat{g}(\mathbf{x}, \mathbf{x}')$ via (1) by using g_0 , γ , and $\hat{s}(\mathbf{x}, \mathbf{x}')$
-

$$\begin{aligned} H_t &:= H(\mathbf{f}|\tilde{\mathbf{s}}_t, \mathbf{z}, \boldsymbol{\theta}) = \sum_{\mathbf{z}' \in \mathcal{Z}} \int_{\tilde{\mathbf{s}}'_t, \boldsymbol{\theta}'} p(\tilde{\mathbf{s}}'_t, \mathbf{z}', \boldsymbol{\theta}') \\ &\quad \times H(\mathbf{f}|\tilde{\mathbf{s}}_t = \tilde{\mathbf{s}}'_t, \mathbf{z} = \mathbf{z}', \boldsymbol{\theta} = \boldsymbol{\theta}') d\boldsymbol{\theta}' d\tilde{\mathbf{s}}'_t \end{aligned} \quad (14)$$

where $H(\mathbf{f}|\tilde{\mathbf{s}}_t = \tilde{\mathbf{s}}'_t, \mathbf{z} = \mathbf{z}', \boldsymbol{\theta} = \boldsymbol{\theta}') := - \int p(\mathbf{f}|\tilde{\mathbf{s}}'_t, \mathbf{z}', \boldsymbol{\theta}') \times \ln p(\mathbf{f}|\tilde{\mathbf{s}}'_t, \mathbf{z}', \boldsymbol{\theta}') d\mathbf{f} = (\ln |\boldsymbol{\Sigma}_{\mathbf{f}|\mathbf{z}'}| + N_g(1 + \ln 2\pi))/2$ and $|\cdot|$ denotes matrix determinant. To obtain $\tilde{\mathbf{s}}_{t+1}$, one can choose a pair of sensors, or equivalently find \mathbf{w}_{t+1} , minimizing $H(\mathbf{f}|\tilde{\mathbf{s}}_{t+1}, \mathbf{z}, \boldsymbol{\theta})$. Once expressing $H_{t+1} = H_t - \sum_{\mathbf{z}' \in \mathcal{Z}} \int_{\tilde{\mathbf{s}}'_{t+1}, \boldsymbol{\theta}'} p(\tilde{\mathbf{s}}'_{t+1}, \mathbf{z}', \boldsymbol{\theta}') q(\mathbf{z}', \boldsymbol{\theta}', \mathbf{w}_{t+1}) d\boldsymbol{\theta}' d\tilde{\mathbf{s}}'_{t+1}$ with $q(\mathbf{z}, \boldsymbol{\theta}, \mathbf{w}) := \ln(1 + (\sigma_v^2)^{-1} \mathbf{w}^\top \boldsymbol{\Sigma}_{\mathbf{f}|\mathbf{z}} \mathbf{w})/2$ by use of the matrix determinant identity lemma [24, Chapter 18], given $\tilde{\mathbf{s}}_t = \tilde{\mathbf{s}}'_t$, it yields \mathbf{w}_{t+1} as the solution of

$$\begin{aligned} (\text{P1}) \quad &\max_{\mathbf{w} \in \mathcal{W}_{t+1}} \mathbb{E}_{\mathbf{z}, \boldsymbol{\theta}|\tilde{\mathbf{s}}_t = \tilde{\mathbf{s}}'_t} [q(\mathbf{z}, \boldsymbol{\theta}, \mathbf{w})] \\ &= \sum_{\mathbf{z}' \in \mathcal{Z}} \int_{\boldsymbol{\theta}'} p(\mathbf{z}', \boldsymbol{\theta}'|\tilde{\mathbf{s}}_t = \tilde{\mathbf{s}}'_t) q(\mathbf{z}', \boldsymbol{\theta}', \mathbf{w}) d\boldsymbol{\theta}' \end{aligned} \quad (15)$$

where \mathcal{W}_{t+1} is a set of weight vectors found from locations of available sensing radio pairs at time slot $t + 1$.

Although (P1) can be solved in a greedy fashion when $\boldsymbol{\theta}$ is fixed as in this work, evaluating $\mathbb{E}_{\mathbf{z}, \boldsymbol{\theta}|\tilde{\mathbf{s}}_t = \tilde{\mathbf{s}}'_t} [q(\mathbf{z}, \boldsymbol{\theta}, \mathbf{w})]$ is still intractable for large N_g since $|\mathcal{Z}| = 2^{N_g}$. Fortunately, the samples from Alg. 1 help to approximate

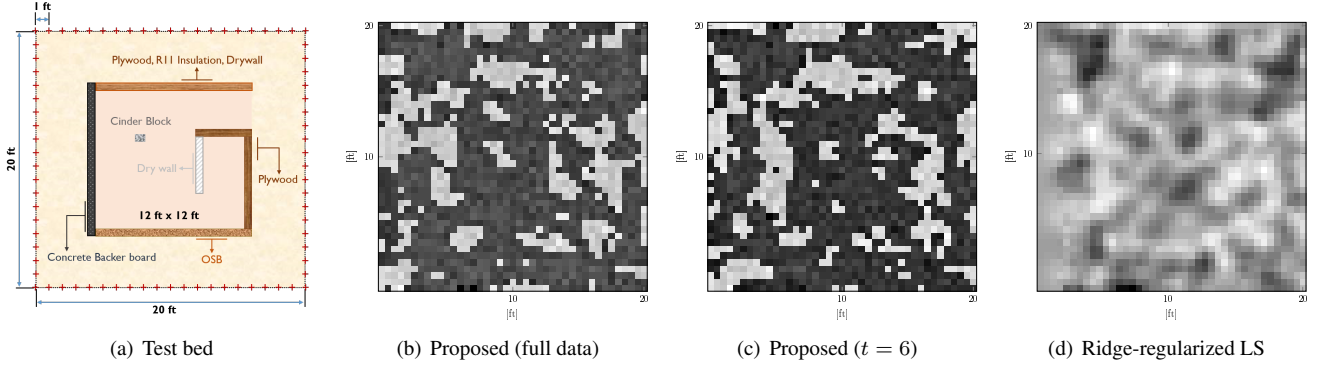


Fig. 1. Configuration of the test bed, and SLF reconstructions by the proposed and ridge-regularized LS methods.

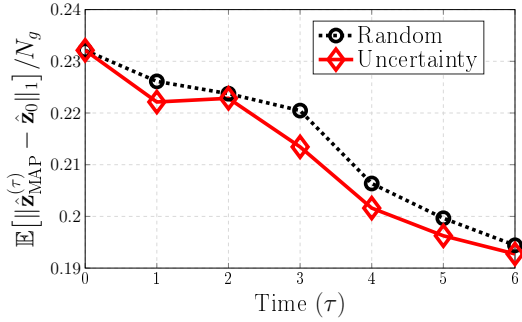


Fig. 2. Estimation error of z versus time slots.

$$\mathbb{E}[q(z, \theta, \mathbf{w})] \simeq \frac{1}{|\mathcal{S}|} \sum_{l=N_{\text{Burn}}+1}^{N_{\text{Iter}}} q(z^{(l)}, \theta^{(l)}, \mathbf{w}) =: \bar{u}(\mathbf{w}). \quad (16)$$

Therefore, \tilde{s}_{t+1} can be obtained from the pair of sensors corresponding to \mathbf{w} with the maximum value of $\bar{u}(\mathbf{w})$ in (16). Note that the proposed adaptive sampling scheme can be easily extended to the case of the mini-batch of size N_{Batch} by finding weight vectors associated with N_{Batch} largest values of $\bar{u}(\mathbf{w})$ in (16).

The overall algorithm for adaptive Bayesian CG cartography is tabulated in Alg. 3.

4. NUMERICAL TESTS

This section describes numerical tests using the real data of [12] to validate the performance of the proposed framework for CG cartography. The test bed is depicted in Fig. 1(a), where $\mathcal{A} = [0.5, 20.5]^2$ is a square with sides of 20 feet (ft), over which a grid $\{\tilde{\mathbf{x}}_i\}_{i=1}^{N_g} := \{1, 41\}^2$ of $N_g = 1,681$ points is defined. A collection of $N = 80$ sensors measure the channel attenuation at 2.425 GHz between pairs of sensor positions, marked with the crosses. To estimate g_0 and γ in (1) using the approach in [12], a first set of 2,400 measurements was obtained before placing the artificial structure in Fig. 1(a). Afterwards, the structure in Fig. 1(a) was assembled, and $\{g_\tau\}_{\tau=1}^{2,380}$ were obtained and calibrated to obtain measurements $\tilde{\mathbf{s}}_t = [\tilde{s}_1, \dots, \tilde{s}_{2,380}]^\top$.

To test the proposed algorithm, $\{\mathbf{w}_\tau\}$ were constructed with w in (3); Alg. 3 was initialized with $\mathbf{z}^{(0)}$ randomly drawn from $\{0, 1\}^{N_g}$, and 1,000 measurements for $\tilde{\mathbf{s}}_0$ chosen uni-

formly at random. The remaining 1,380 measurements were used to test Alg. 3. Other parameters were set to $\sigma_v^2 = 64$, $\beta = 2.73$, and $\theta_f = [0, 0.3, 10^{-1}, 10^{-1}]^\top$, $N_{\text{Burn}} = 60$, and $N_{\text{Iter}} = 250$, throughout the simulated tests. Per time slot t , \mathcal{W}_t was found by weight vectors associated with 150 measurements chosen uniformly at random, from the remaining 1,380 measurements without replacement, and then $N_{\text{Batch}} = 100$ measurements were collected. As a competing alternative, the ridge-regularized LS estimator $\hat{\mathbf{f}}_{\text{LS}} = (\mathbf{W}_t \mathbf{W}_t^\top + \omega \mathbf{C}_f^{-1})^{-1} \mathbf{W}_t \tilde{\mathbf{s}}_t$ was also tested [12], where ω is a regularization parameter and \mathbf{C}_f is a spatial covariance matrix modeling the similarity between points \mathbf{x} and \mathbf{x}' as $\mathbf{C}_f(\mathbf{x}, \mathbf{x}') = \sigma_s^2 \exp[-\|\mathbf{x} - \mathbf{x}'\|_2 / \kappa]$ [6], with $\sigma_s^2 = \kappa = 1$, and $\omega = 79.9$; see also [11].

Fig. 1(c) depicts the reconstructed SLF by Alg. 3 at $t = 6$, or with 1,600 measurements. Comparison with the SLF reconstructed with the full data (2,380 measurements) in Fig. 1(b) demonstrates the effectiveness of the proposed algorithm in identifying the structure of the propagation medium with adaptively chosen fewer measurements. The blurry image of the SLF in Fig. 1(d) reconstructed by the ridge-regularized LS with 1,600 measurements chosen uniformly at random showcases the benefit of adopting the Gauss-Potts model for CG cartography.

Efficacy of the adaptive data acquisition method was also validated by measuring the estimation error of z as $\|\hat{\mathbf{z}}_{\text{MAP}}^{(t)} - \hat{\mathbf{z}}_0\|_1 / N_g$, where $\hat{\mathbf{z}}_0$ is the estimate of z with the full data. Fig. 2 displays the estimation error of z by Alg. 3 with random and uncertainty sampling methods, obtained by averaging the error over 10 independent Monte Carlo runs. This plot illustrates that higher estimation accuracy is achievable by adaptively collecting fewer samples.

5. CONCLUDING SUMMARY

This paper developed a novel adaptive Bayesian channel gain cartography algorithm capable of constructing maps that provide the channel gain between arbitrary locations in a region of interest while revealing the structure of the propagation medium through a spatial loss field, equipped with adaptive data acquisition capability. Efficacy of the novel algorithm was validated through real data tests.

6. REFERENCES

- [1] S.-J. Kim, E. Dall'Anese, and G. B. Giannakis, "Co-operative spectrum sensing for cognitive radios using kriged Kalman filtering," *IEEE J. Sel. Topics Sig. Process.*, vol. 5, no. 1, pp. 24–36, Feb. 2011.
- [2] E. Axell, G. Leus, and E. G. Larsson, "Overview of spectrum sensing for cognitive radio," in *Proc. Cognitive Inf. Process.*, 2010, pp. 322–327.
- [3] Q. Zhao and B. M. Sadler, "A survey of dynamic spectrum access," *IEEE Sig. Process. Mag.*, vol. 24, no. 3, pp. 79–89, 2007.
- [4] Federal Communications Commission, "FCC 11-131," *Unlicensed Operation in the TV Broadcast Bands*, 2011.
- [5] S.-J. Kim, E. Dall'Anese, J. A. Bazerque, K. Rajawat, and G. B. Giannakis, "Advances in spectrum sensing and cross-layer design for cognitive radio networks," in *Academic Press Library in Signal Processing: Communications and Radar Signal Processing: 2*, chapter 9, pp. 471–497. Academic Press, 2013.
- [6] P. Agrawal and N. Patwari, "Correlated link shadow fading in multi-hop wireless networks," *IEEE Trans. Wireless Commun.*, vol. 8, no. 9, pp. 4024–4036, Aug. 2009.
- [7] N. Patwari and P. Agrawal, "Effects of correlated shadowing: Connectivity, localization, and RF tomography," in *Int. Conf. Info. Process. Sensor Networks*, St. Louis, MO, Apr. 2008, pp. 82–93.
- [8] J. Wilson and N. Patwari, "Radio tomographic imaging with wireless networks," *IEEE Trans. Mobile Comput.*, vol. 9, no. 5, pp. 621–632, 2010.
- [9] J. Wilson and N. Patwari, "See-through walls: Motion tracking using variance-based radio tomography networks," *IEEE Trans. Mobile Comput.*, vol. 10, no. 5, pp. 612–621, 2011.
- [10] E. Dall'Anese, S.-J. Kim, and G. B. Giannakis, "Channel gain map tracking via distributed kriging," *IEEE Trans. Veh. Technol.*, vol. 60, no. 3, pp. 1205–1211, 2011.
- [11] D. Lee, S.-J. Kim, and G. B. Giannakis, "Channel gain cartography for cognitive radios leveraging low rank and sparsity," *IEEE Trans. Wireless Commun.*, vol. 16, no. 9, pp. 5953 – 5966, Nov. 2017.
- [12] B. R. Hamilton, X. Ma, R. J. Baxley, and S. M. Metchik, "Propagation modeling for radio frequency tomography in wireless networks," *IEEE J. Sel. Topics Sig. Proc.*, vol. 8, no. 1, pp. 55–65, Feb. 2014.
- [13] D. Romero, D. Lee, and G. B. Giannakis, "Blind channel gain cartography," in *Proc. 2016 IEEE Global Conf. on Signal and Info. Process.*, Washington, D.C., Dec. 2016, pp. 1110–1115.
- [14] J. Wilson and N. Patwari, "Radio tomographic imaging with wireless networks," *IEEE Trans. Mobile Comput.*, vol. 9, no. 5, pp. 621–632, Jan. 2010.
- [15] D. Higdon, *Spatial applications of Markov chain Monte Carlo for Bayesian inference*, Ph.D. thesis, Dept. Stat., Univ. Washington, Seattle, WA, 1994.
- [16] W. R. Gilks, S. Richardson, and D. J. Spiegelhalter, *Markov Chain Monte Carlo in Practice*, Chapman and Hall, London, 1996.
- [17] D. Smith and M. Smith, "Estimation of binary Markov random fields using Markov chain Monte Carlo," *J. Comput. Graph. Stats.*, vol. 15, no. 1, pp. 207 – 227, 2006.
- [18] J. Hammersley and P. Clifford, "Markov field on finite graphs and lattices," Unpublished manuscript, 1971.
- [19] H. Ayasso and A. Mohammad-Djafari, "Joint NDT image restoration and segmentation using Gauss-Markov-Potts models and variational Bayesian computation," *IEEE Trans. Image Process.*, vol. 19, no. 9, pp. 2265 – 2277, Sep. 2010.
- [20] G. Kail, J.-Y. Tournet, F. Hlawatsch, and N. Dobiigeon, "Blind deconvolution of sparse pulse sequences under a minimum distance constraint: a partially collapsed Gibbs sampler method," *IEEE Trans. Sig. Proc.*, vol. 60, no. 6, pp. 2727 – 2743, 2012.
- [21] N. Zhao, A. Basarab, D. Kouamé, , and J.-Y. Tournet, "Joint segmentation and deconvolution of ultrasound images using a hierarchical Bayesian model based on generalized Gaussian priors," *IEEE Trans. Image Process.*, vol. 25, no. 8, pp. 3736 – 3750, 2016.
- [22] D. MacKay, "Information-based objective functions for active data selection," *Neural Comput.*, vol. 4, no. 4, pp. 590 – 604, 1992.
- [23] T. M. Cover and J. A. Thomas, *Elements of Information Theory*, USA:Wiley, New York, NY, 1991.
- [24] D. A. Harville, *Matrix Algebra From a Statistician's Perspective*, Springer-Verlag, New York, NY, 1997.